AN UNSPLIT GRP METHOD FOR 2D COMPRESSIBLE FLOW ON A CURVILINEAR GRID

L. Wang[1], J. Falcovitz[2], O. Igra[1] and G. Ben-Dor[1]

1) The Pearlstone Center for Aeronautical Engineering Studies, Department of Mechanical Engineering, Ben-Gurion University of the Negev, Beer Sheva, Israel
2) Faculty of Aerospace Engineering, Technion, I.I.T., Haifa, Israel

Abstract

The paper describes an unsplit Generalized Riemann Problem (GRP) method for solving numerically the equations governing time-dependent compressible flow in two space dimensions. Unstructured curvilinear grids are used for efficient treatment of flows subjected to complex geometrical boundary conditions. The time-integration of the hydrodynamic conservation laws consists of two distinct phases. First, cell-interface fluxes are computed using analytical solutions to Generalized Riemann Problems resolving discontinuities in flow and flow gradients between discretised approximations at adjacent cells. Second, these fluxes are used in a finite-volume scheme to integrate the hydrodynamic conservation laws by a single time-step in each cell. The versatility and robustness of the method are demonstrated by treating complex shock reflections from airfoils at high angles of attack. Solutions exhibit a high degree of resolution of shock and contact discontinuities. It is concluded that the method shows promise in handling complex flow fields arising from shock wave diffraction phenomena, combining the features of high resolution and scheme robustness.

Introduction

Shock wave diffraction around airfoils at a high angle of attack results in complex flow features. Mandella and Bershader[1] investigated the unsteady process in a shock tube experiment. A schematic description of their experimental apparatus and the investigated flow field are shown in Fig. 1. In the recent study by Lee and Bershader[2] the same experimental setup was used as the first step in studying head-on parallel blade-vortex interaction. An NACA 0018 airfoil at angle of attack of 30^{o} around which the shock wave diffracts was used as a vortex generator. At the trailing edge of the airfoil a two-dimensional shock-induced starting vortex was generated and convected downstream to interact with a target NACA 0012 airfoil. Moon & Yee[3] and Young and Yee[4] simulated numerically the shock wave diffraction around an airfoil using a TVD scheme.

The present paper describes an unsplit GRP method for two-dimensional compressible flow around airfoils. It uses a curvilinear grid to simulate the complex flow resulting from shock wave diffraction around the airfoil.

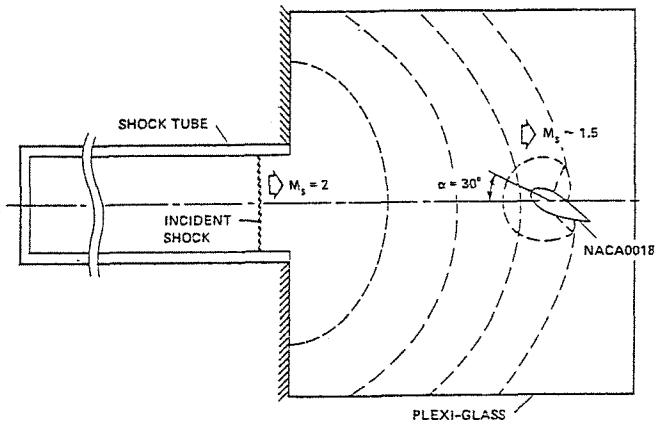

Fig. 1 Illustration of the facility used for studying experimentally the shock wave interaction with an airfoil.

The Generalized Riemann Problem (GRP) scheme was originally proposed by Ben-Artzi and Falcovitz[5] for compressible quasi-one-dimensional duct flows and was later extended to multi-dimensional flows employing Strang's operator splitting; at present it was applied to more complex flow problems[6,7,8]. The method described subsequently pursues a finite-volume form for the integration of the conservation laws and body-fitting coordinates. An advantage of this technique is in the relatively easy implementation of the flow boundary conditions. An unstructured data organization is adopted to cope with the complex flow simulation.

In the following the main features of the numerical scheme are given and the kernel steps needed for solving a Generalized Riemann Problem are outlined.

Numerical Method

The Euler equation may be written in two-dimensional conservation form as

$$\frac{\partial U}{\partial t}+\frac{\partial F}{\partial x}+\frac{\partial G}{\partial y}=0 \qquad (1)$$

It consists of four equations expressing conservation of mass, momentum in the x and y directions, and energy of the fluid. In Eq. (1) U is the state vector expressing the variables of density, the two-components of momentum and the total energy. The vectors F and G represent the

convective fluxes. The equations are integrated over an area S as

$$\iint_S \frac{\partial U}{\partial t} dS + \iint_S \left(\frac{\partial F}{\partial x} + \frac{\partial G}{\partial y} \right) dS = 0 \qquad (2)$$

The integration of the second integral appearing in Eq. (2) is evaluated using Green's theorem,

$$\frac{\partial}{\partial t} \iint_S U dS + \oint \left(Fn_x + Gn_y \right) dL = 0 \qquad (3)$$

The flow domain is divided into a collection of quadrilateral cells. Equation (3) is considered for each one of the cells and the averaged values of the state vector in cell i obeys a partially discretised ordinary difference equation as follows:

$$S_i \left(\frac{dU}{dt} \right)_i = -\sum_{i=1}^{4} \left(Fn_x + Gn_y \right) \Delta L_{on-cell-edge} \qquad (4)$$

here $\sum_{i=1}^{4}$ means summation of fluxes over the four sides of the i-th cell and the flux functions ($Fn_X + Gn_Y$) on the cell edges are obtained by solving a Generalized Riemann Problem arising at the cell boundaries from a piecewise approximation of the flow in each cell. GRP initial conditions include jumps in flow gradients as well as flow variables. Local characteristic analysis for the GRP leads to a solution for the primitive physical variables at the cell boundary to a second-order accuracy which is subsequently used in a conservation law scheme, producing a high resolution shock capturing capability and also second-order accuracy in the region of smooth flows.

The grid generation is conducted in the following manner. First an algebraic grid generation method is used to generate a C-type grid around the airfoil as shown in Fig. 2a. All the data are stored in a matrix form, i.e., x(i,j), y(i,j), etc. Then the flow domain is specified as a rectangular with the airfoil positioned at about its center. A reorganization procedure is carried out that rotates the same angle as the angle of attack of the airfoil and records all the data for the cells within the rectangular domain into a one-dimensional array. All others, not in the domain are excluded. The flow domain with unstructured data organization is shown in Fig. 2b having a feature of zig-zag boundaries, on which the computation is to be conducted.

Numerical Results

A description of the physical problem to be computed is shown in Fig. 3. A planar shock wave of Mach number 1.5 moves towards an NACA 0018 airfoil positioned at an angle of attack of 30°. This is an approximation to the flow conditions existing at the moment of impingement of a diffracted curved shock wave with the airfoil in

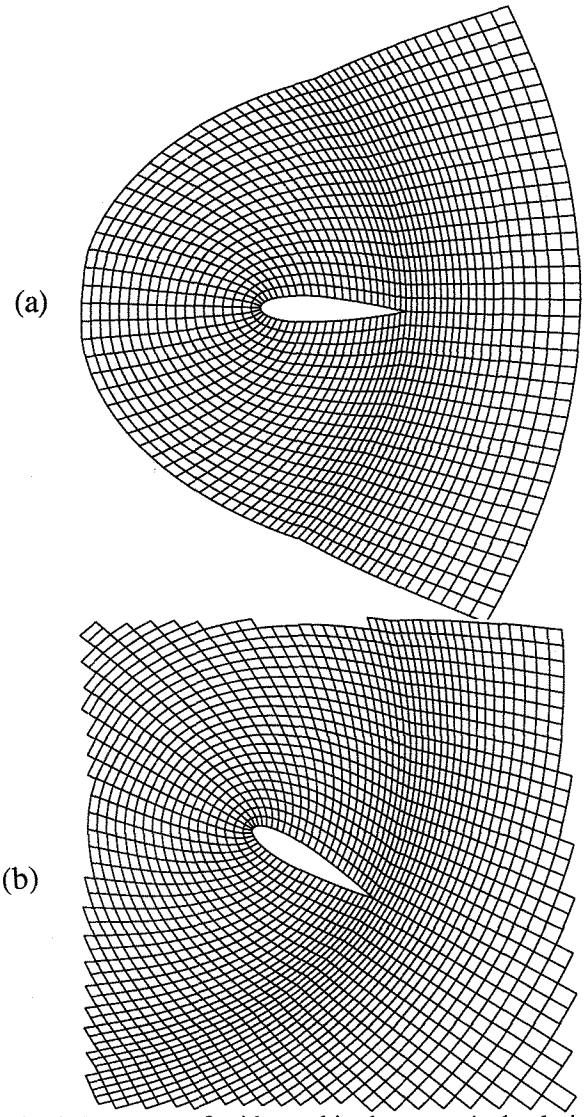

Fig. 2 Geometry of grids used in the numerical solution.

Mandella and Bershader's experiment[1]. The ambient pressure and temperature are set at 1 atm and 15°C, respectively. The initial condition is obtained from the Rankine-Hugoniot shock relations. Along the upper and lower boundaries of the flow domain the planar shock wave condition is applied for tracing the leading shock wave. Along the upstream (or downstream) boundary an Inflow (or outflow) condition is implemented. A solid wall condition is imposed along the airfoil surface.

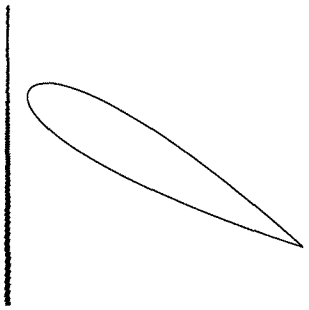

Fig. 3 Schematic description of the investigated flow field prior to the collision between the planar shock wave and the airfoil.

We define here a dimensionless time $\tilde{t}$, $\tilde{t} = \frac{t}{L} a_\infty$, and coordinates $(\tilde{x}, \tilde{y}) = \left(\frac{x}{L}, \frac{y}{L} \right)$ where L is the length of the airfoil chord and a_∞ is the ambient acoustic speed. Initially the incident shock wave is located at a pre-specified distance ahead of the airfoil. We define $\tilde{t} = 0$ as the time when the incident shock wave hits the airfoil and the interaction process starts.

In Fig. 4 five sequential interferograms describing various steps in the shock wave airfoil interaction recorded in shock tube experiments [1] are given. A numerical simulation of this interaction process, at smaller time intervals, is shown in Fig. 5. A sample of distribution curves for the flow Mach number along the airfoil surface for a few of the cases shown in Fig. 5 are given in Fig. 6.

The processes demonstrated by these two sets of results have clear similarities (Figs. 4 and 5). Due to the positive angle of attack of the airfoil on its upper surface close to the leading edge, the flow undergoes a rapid change from compression to expansion. Since the initial flow deflection on the airfoil upper surface, in proximity to the leading edge, is higher than 50^o the incident shock wave will initially reflect as a regular reflection (not shown in Fig. 5). Soon thereafter the reflection will change into a Mach reflection; this type of reflection is clearly shown in Figs. 5a to 5g. The contact surface starting at the triple point (where the incident shock wave, the reflected shock wave and the Mach stem meet) is hardly noticed in the isopicnics shown in Figs. 5a to 5g due to the small density variations through it.

On the lower surface, the fluid is always under compression behind the leading shock wave and the angle between the leading planar shock wave and the tangent of airfoil surface increases monotonicly. Now the transition from a regular to a well-defined single Mach reflection is clearly visible (Figs. 5a, b and c). A very sharp contact surface emanating from the triple point is also visible in Figs. 5b to 5f.

A secondary, back-stream facing, shock wave is formed on the airfoil's upper surface close to its leading edge. This secondary shock wave is needed for matching between the low pressures existing behind the expansion wave, seen just behind the airfoil leading edge, and the high pressure zone which exists behind the lower part of the incident shock wave (Mach stem) on the upper surface of the airfoil (Figs. 5g to 5j). This secondary shock wave terminates the supersonic flow pocket which exists on the airfoil's upper surface behind its leading edge. The formation of this secondary shock wave and the supersonic flow pockets which ends at this shock is easily detectable in Fig. 6 where the flow Mach number distribution around the airfoil is shown. In Fig. 6a the supersonic pockets terminate by a back-stream facing compression wave. At a later time (Fig. 6b) this compression wave coalesces into a well-formed shock wave.

At about $\tilde{t} = 0.55$ after the impingement of the incident shock wave on the airfoil, the Mach stem on the lower surface starts to diffract around the sharp trailing

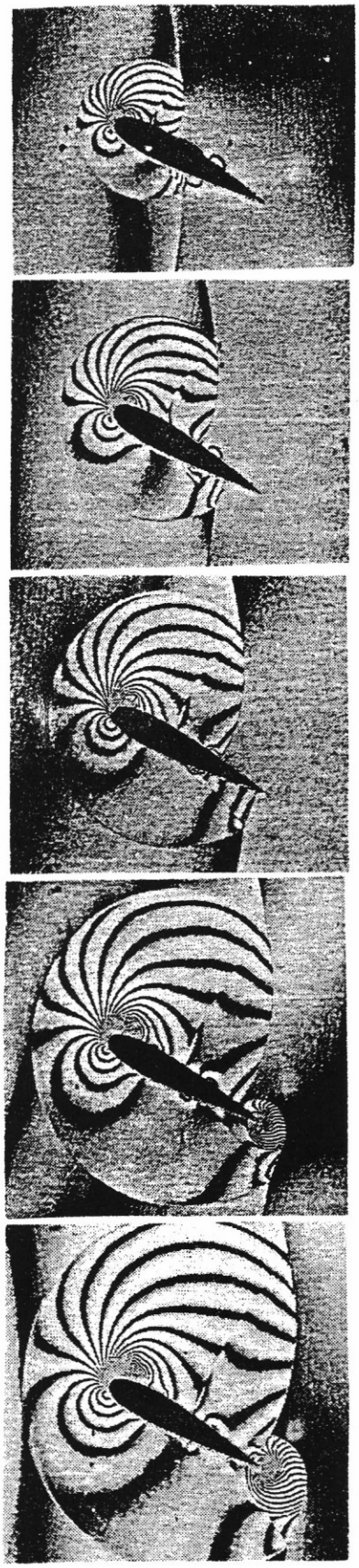

Fig. 4 Interferograms (taken from Ref. 1) showing various time steps during the shock wave interaction with an NACA 0018 airfoil.

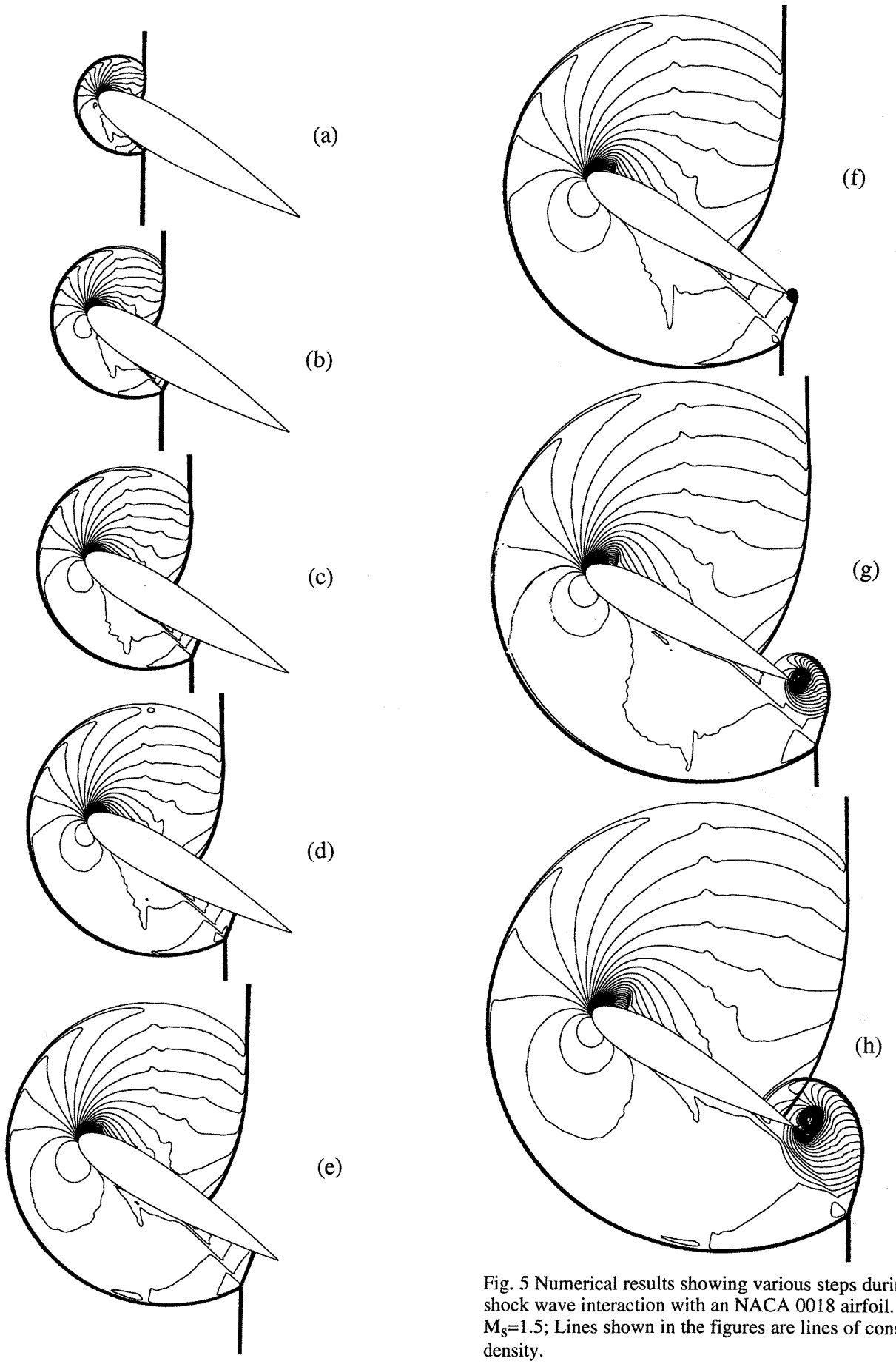

Fig. 5 Numerical results showing various steps during the shock wave interaction with an NACA 0018 airfoil. M_S=1.5; Lines shown in the figures are lines of constant density.

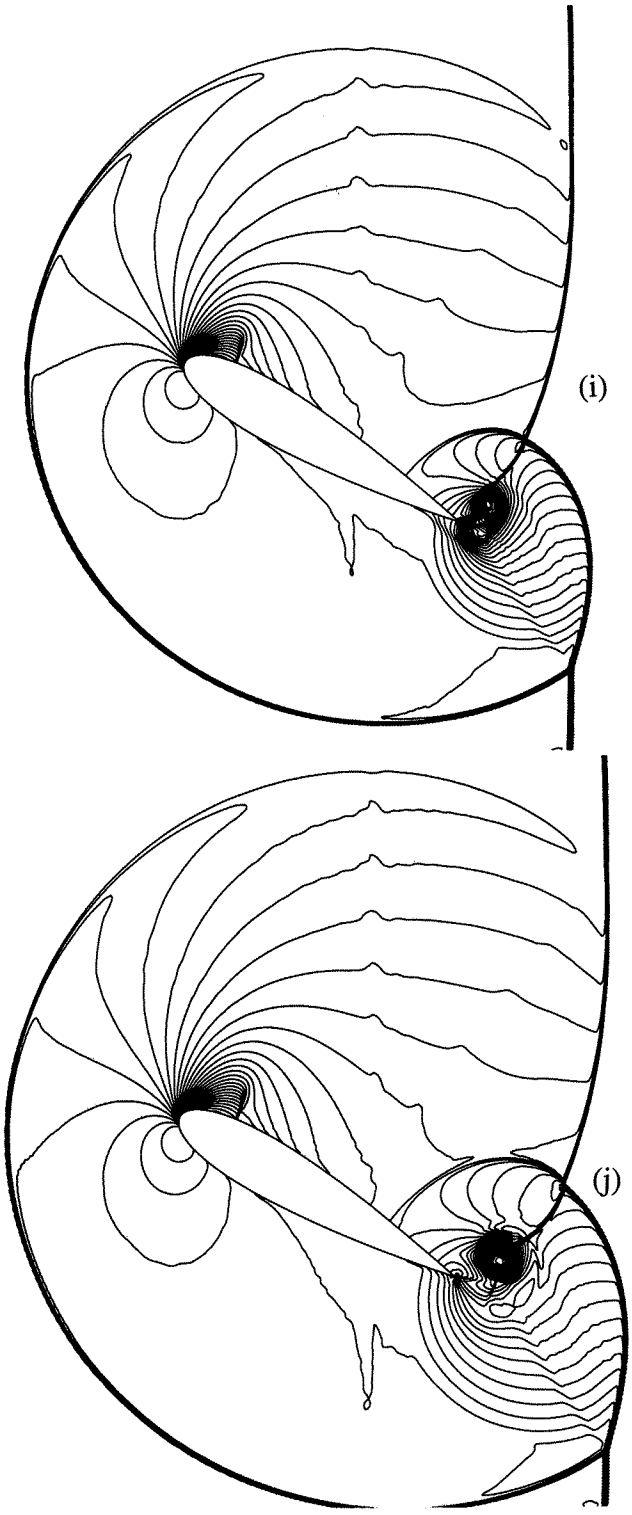

Fig. 5 Continue from previous page.

edge (Fig. 5f). Due to the subsonic flow behind the Mach stem and the rapid flow expansion around the sharp trailing edge, a well-defined shock-induced starting vortex is formed there (see Fig. 5g). The Mach stem continually wraps around, moves forward and interacts with the downward moving curved shock wave on the airfoil's upper surface (Fig. 5h). The interacting pattern is first regular and finally develops into an irregular interaction at about $\tilde{t} = 0.89$ (Fig. 5j). The lower branch of the curved shock wave interacts with the induced vortex and then knocks it off the airfoil surface, see Fig. 5j.

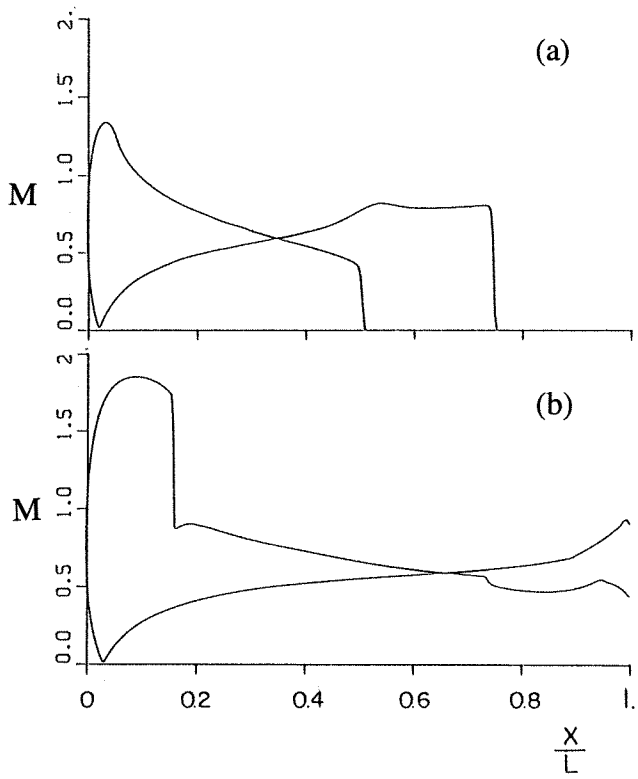

Fig. 6 Flow Mach number distribution along the airfoil's surfaces.

Additional calculations were conducted for a much stronger incident shock wave i.e., one for which $M_S = 8$. The obtained results are shown in Fig. 7. In the computations, results of which are shown in Fig. 7, the equation of state for a perfect gas was used with one change; the ratio of specific heats, γ was altered from 1.4 to $\gamma = 1.35$. This run was conducted mainly in order to show the robustness of the proposed method in simulating high Mach number flows without tuning or readjusting the parameters or schemes. Of course, for an accurate simulation of such a high Mach number flow, real gas effect must be accounted for. Comparing the results shown in Fig. 7 with those of Fig. 5 clearly shows that the secondary shock wave in the former (Fig. 7) is further away from the airfoil's leading edge than in Fig. 5. Furthermore, complex Mach reflection forms on the lower surface (Fig. 7a). Due to the supersonic flow behind the incident shock wave, the flow undergoes a Prandtl-Mayer expansion around the airfoil's trailing edge rather than a vortex-forming expansion as was the case before (Fig. 5). In the present case (Fig. 7) another secondary shock wave forms to terminate the expansion fan around the trailing edge and match it with the lower speed and higher pressure flow behind the diffracted Mach stem.

All computations are performed with a Silicon Graphics Crimson IRIX 4.0.5 computer. The total number of cells covering the flow domain is about 170,000. The above-presented results clearly show the

high resolution of the method in capturing all complex flow features and the robustness of the code.

Conclusion

The paper describes a finite volume Generalized Riemann Problem method for solving numerically a two-dimensional, inviscid compressible flow. Unstructured curvilinear grids are used for efficient treatment of flows subjected to complex geometrical boundary conditions. The versatility and robustness of the method are demonstrated by treating complex shock wave reflections from airfoils at high angles of attack. The obtained solutions exhibit a high degree of resolution in capturing shock and contact discontinuities. A comparison between experiments (interferograms) and numerically obtained isopicnics confirms the reliability of the present numerical results. It is concluded that the method shows promise in handling complex flow fields arising from shock wave diffraction phenomena, combining the feature of high resolution and scheme robustness.

Reference

1. M. Mandella and D. Bershader, "Quantitative Study of Compressible Vortices: Generation, Structure and Interaction with Airfoil," AIAA Paper No. 87-0328, Jan. 1987.
2. S. Lee and D. Bershader, "Head-on Parallel Blade Vortex Interaction," AIAA J., Vol. 32, No. 1, Jan. 1994.
3. Y.J. Moon and H.C. Yee, "Numerical Simulation by TVD Schemes of Complex Shock Reflections from Airfoils at High Angle of Attack," AIAA Paper No. 87-0350, Jan. 1987.
4. V.Y.C. Young and H.C. Yee, "Numerical Simulation of Shock Wave Diffraction by TVD Schemes," AIAA Paper No. 87-0112, Jan. 1987.
5. M. Ben-Artzi and J. Falcovitz, "An Upwind Second-Order Scheme for Compressible Duct Flows," SIAM Journal on Scientific Statistical Computing, Vol. 7, pp. 744-768, 1986.
6. J. Falcovitz, O. Igra, L. Wang, W. Heilig and H. Reichenbach, "The Interaction of Normal Shock Wave with a Square Trench," presented at the 19th Int. Symp. on Shock Waves, Université de Provence, Marseille, France, July 26-30, 1993.
7. J. Falcovitz, G. Ben-Dor, G. Alfandary, "Numerical and Experimental Study of a Head-On Reflection of a Regular Reflection", Int. J. of Numerical Methods in Fluids, Vol. 17, pp. 1055-1077, 1993.
8. J. Falcovitz, G. Alfandary and G. Hanoch, "Moving Boundary Tracking in Compressible Flow Computation," JSME Spring Annual Meeting, March 29-31, 1994, Tokyo, Japan.

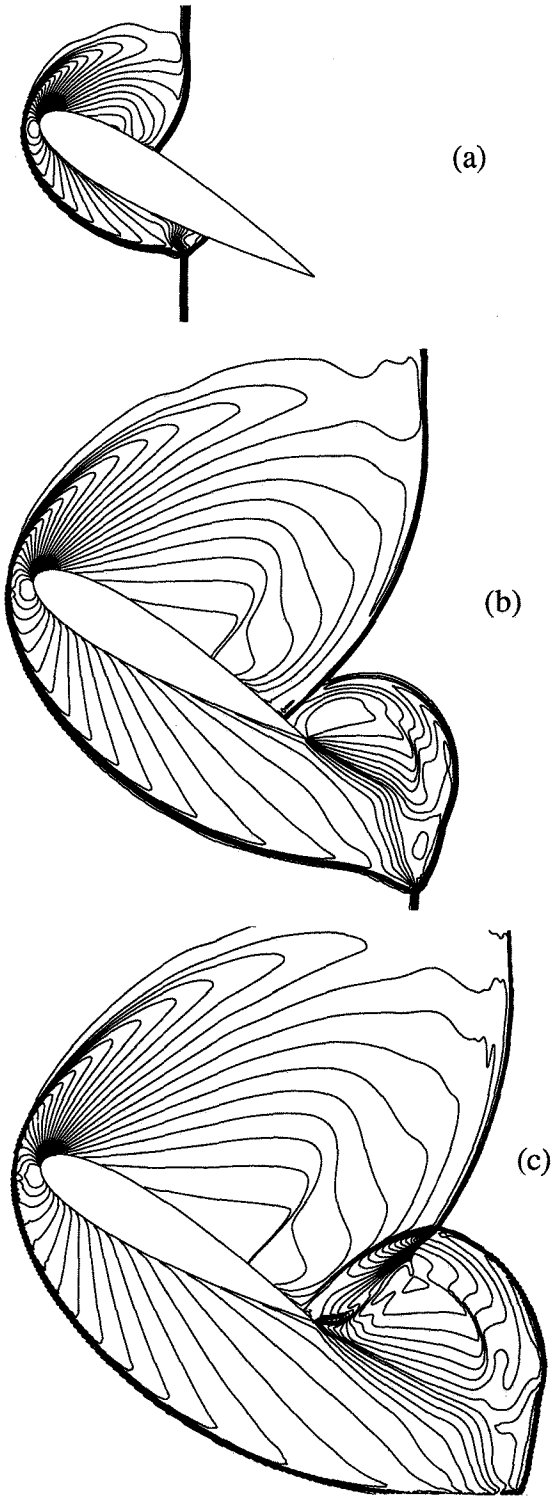

Fig. 7 Numerical results showing various steps during the interaction of a strong shock wave (M_S=8) with an NACA 0018 airfoil. Lines shown in the figures are lines of constant density.